DOI: 10.1002/ ((please add manuscript number))
Article type: Full Paper

Multi-functional Coatings from Scalable Single Source Precursor Chemistry in Tandem Photoelectrochemical Water Splitting

*Yi-Hsuan Lai, David W. Palm and Erwin Reisner,**

Dr. Y.-H. Lai, D. W. Palm, Dr. E. Reisner
Christian Doppler Laboratory for Sustainable SynGas Chemistry, Department of Chemistry, University of Cambridge, Cambridge CB2 1EW, UK.
E-mail: reisner@ch.cam.ac.uk; website: http://www-reisner.ch.cam.ac.uk

Keywords: nanocomposite materials; photocatalysis, photoelectrochemistry, solar energy, water splitting

Abstract

The straightforward and inexpensive fabrication of stabilized and activated photoelectrodes for application in tandem photoelectrochemical (PEC) water splitting is reported. Semiconductors such as Si, WO_3 and $BiVO_4$ can be coated with a composite layer formed upon hydrolytic decomposition of heterobimetallic single source precursors (SSPs) based on Ti and Ni or Ti and Co in a simple single-step process under ambient conditions. The resulting 3d-transition metal oxide composite films are multi-functional, as they protect the semiconductor electrode from corrosion with an amorphous TiO_2 coating and act as bifunctional electrocatalysts for H_2 and O_2 evolution based on catalytic Ni or Co species. Thus, this approach enables the use of the same precursors for both photoelectrodes in tandem PEC water splitting, and SSP chemistry is thereby established as a highly versatile low-cost approach to protect and activate photoelectrodes. In an optimized system, SSP coating of a Si photocathode and a $BiVO_4$ photoanode resulted in a benchmark noble-metal free dual-photoelectrode tandem PEC cell for overall solar water splitting with an applied bias solar-to-hydrogen efficiency of 0.59% and a half-life photostability of five hours.

1. Introduction

Solar-driven water splitting is an attractive technological concept for the generation of sustainable H_2 fuel from sunlight and water.[1] A photoelectrochemical (PEC) cell is a promising device for fulfilling this purpose because its capital cost may potentially be lower than that of an electrolyzer wired to photovoltaic (PV) modules, and it has an attractive theoretical efficiency.[2] The upper limit efficiency of a tandem PEC cell with a pair of semiconductors having band gaps of 1.0 and 1.6 eV is close to 30%,[3] whereas only 13% is achievable for a single light absorber PEC cell consisting of a semiconductor with a band gap of 2.2 eV.[2c]

Several designs of tandem PEC cells are currently under investigation.[4] For example, tandem cells that use a single dual-absorbing photoelectrode paired with an expensive platinum counter electrode,[5] or PVs integrated with a photoelectrode are widely studied.[4a-c] In contrast, studies of tandem PEC cells that pair a photoanode with a photocathode are still limited (**Figure 1**).[6] Toward this goal, immense efforts have been devoted to optimize the performance of individual photoelectrodes by interfacing them with protection layers to enhance photostability and by integrating electrocatalysts for more efficient fuel-formation.[1a, 7] In addition, major challenges arise from the incompatibility between photoanode and photocathode materials, electrolyte solutions, integrated catalysts and/or other elements.[1a, 2a] A simple, cost-effective, and universal process to protect and activate the photoelectrodes and make them compatible with each other would therefore be very beneficial.

Protection of promising but photo-unstable electrode materials with a stable and conducting layer such as amorphous TiO_2 is an attractive approach to enhance their lifetime during operation in a PEC cell. However, these protection layers are typically prepared by costly atomic layer deposition (ALD)[7d, 8] or sputtering technologies,[9] which are challenging to scale up. In order to enhance photocatalytic performance, electrocatalysts are integrated onto

semiconductor electrodes that exhibit low photocurrent densities.[7a, 7b] The bifunctional water splitting electrocatalysts can promote both the hydrogen and oxygen evolution reactions, and are an interesting approach for minimizing the complexity and cost of integrated water splitting systems.[10] However, such bifunctional catalysts have only been reported for water electrolysis, and their preparation has required electrodeposition and chemical synthesis, which have thus far prevented their simple integration in a PEC system.

Solution processed single source precursor (SSP) chemistry is an attractive approach for preparing multi-functional materials on a large scale, as it bypasses the need for expensive equipment and processing.[11] A SSP contains all of the required elements for a desired composite material, allowing for its synthesis in a simple, one-step procedure. In addition, the material prepared from a SSP can comprise novel composite phases and oxidation states, which might be difficult to achieve with conventional synthetic routes.[11a, 11e]

Herein, we report on a highly versatile and scalable SSP approach for preparing a composite film on photoelectrodes. This composite is multi-functional, serving three main purposes: it protects the photoelectrode from corrosion and can act as both a hydrogen evolution catalyst (HEC) and an oxygen evolution catalyst (OEC) in the same neutral-alkaline solution. Thus, individual photoelectrodes coated with the SSPs can also be arbitrarily combined in tandem PEC cells. The SSPs employed in this study are $[Ti_2(OEt)_9(NiCl)]_2$ ($TiNi_{SSP}$) and $[Ti_4O(OEt)_{15}(CoCl)]$ ($TiCo_{SSP}$) (**Figure 2**).[12] $TiNi_{SSP}$ and $TiCo_{SSP}$ were selected firstly because their hydrolysis forms amorphous TiO_2, which is inexpensive and the most widely used protective coating on photoelectrodes that suffer from severe instability.[7d, 9] Furthermore, decomposition of the SSPs will form Ni[7d, 10a, 10b, 13] and Co[10d, 14] species, which are among the best noble metal-free HECs and OECs and can show bifunctionality for water splitting catalysis.[10] In addition, $TiNi_{SSP}$ and $TiCo_{SSP}$ can be easily synthesized by a single mid-temperature hydrothermal step, with respectable yield.[12] We demonstrate that the

SSPs can be deposited onto Si, WO_3 and $BiVO_4$, where they are activated *in situ* to protect and catalytically activate the semiconductors for both half-reactions in PEC water splitting. Optimized SSP-modified photoelectrodes allowed for the assembly of a benchmark tandem water splitting cell.

2. Results and Discussion

2.1. Electrochemical characterization

The simple coating of the SSPs ($TiNi_{SSP}$ and $TiCo_{SSP}$) onto conducting substrates through room temperature deposition allows for the formation of bifunctional composite materials active as HEC and OEC in a pH 9.2 potassium borate (B_i) solution (**Figure 3**). Hydrolytic decomposition of $TiNi_{SSP}$ (2 x 20 μL, 5 mM in dry toluene) on a fluoride-doped tin oxide (FTO)-coated glass substrate (1 cm^2) has been previously shown to result in an amorphous Ti- and Ni-containing precursor film (FTO|$TiNi_{pre}$).[11a, 11c] Under anodic conditions, a NiO_x OEC embedded in a TiO_2 matrix was formed *in situ* ($TiNi_{OEC}$),[11c] whereas an *in situ* cathodic activation process of the $TiNi_{pre}$ film gave a Ni-based HEC that consists of metallic Ni embedded in an amorphous $NiO/Ni(OH)_2$ and TiO_2 matrix ($TiNi_{HEC}$, Figure 3a).[11a] FTO|$TiNi_{OEC}$ and FTO|$TiNi_{HEC}$ show a catalytic onset potential (E_{cat}) of approximately 1.7 and –0.1 V versus the reversible hydrogen electrode (*vs.* RHE) for O_2 and H_2 evolution, respectively, and Faradaic efficiencies (FEs) of more than 90% for both processes (**Table 1**).

Dropcasting of $TiCo_{SSP}$ (2 x 20 μL, 10 mM in dry toluene) on an FTO-coated glass substrate (1 cm^2) resulted in an amorphous precursor film on FTO (FTO|$TiCo_{pre}$). $TiCo_{pre}$ is a mixture of agglomerated amorphous particles of TiO_2 and $CoO/Co(OH)_2$, which was confirmed by scanning electron microscopy (SEM), powder X-Ray diffraction (p-XRD) and X-ray photoelectron spectroscopy (XPS; Figure S1 and S2). Under an anodic potential, $TiCo_{pre}$ converts *in situ* into $TiCo_{OEC}$, which contains the well-known CoO_x OEC in B_i solution (Figure 3a and S3).[11b, 14d] FTO|$TiCo_{OEC}$ electrooxidizes water to O_2 with an onset

potential of approximately E_{cat} = 1.6 V *vs*. RHE (Figure 3b) and a FE of 88% at an applied potential (E_{appl}) of 2.0 V *vs.* RHE (Table 1 and Figure S3). $TiCo_{HEC}$ forms upon a cathodic activation of $TiCo_{pre}$ at E_{appl} of –0.6 V *vs.* RHE for 10 min, demonstrating the bifunctionality also for TiCo. The current density increased from –1.5 to –3.0 mA cm^{-2} with the formation of H_2 bubbles (confirmed by gas chromatography) during this pre-treatment (Figure S4). The active species of $TiCo_{HEC}$ is presumably similar to a previously reported Co-based HEC, metallic Co with a small portion of $CoO/Co(OH)_2$,[10d] that was prepared by electrodeposition of a Co(II) salt. FTO|$TiCo_{HEC}$ electroreduces protons with an onset potential of approximately E_{cat} = –0.2 V *vs.* RHE and a FE of 92% was observed at E_{appl} = –0.6 V *vs.* RHE (Figure 3b and Table 1).

The current-voltage characteristics and the near-quantitative FE confirm that both $TiNi_{SSP}$ and $TiCo_{SSP}$ act as precursors of HECs and OECs and are therefore rare examples of bifunctional water splitting electrocatalysts.[10a-d] Although the catalytic onset overpotential of these electrocatalysts is somewhat higher than that of other benchmark electrocatalysts, the photocurrent of a photoelectrode during irradiation is not necessarily limited by the non-ideal response of the composite electrocatalysts. Figure 3b indicates the relevant minority-carrier band positions of the semiconductors used in this study, illustrating that a catalyst with a very small overpotential requirement is not necessary for the HEC and OEC to function efficiently in such a PEC system. With respect to the standard potential (E^0) of the appropriate half-reaction, an overpotential (η) of 0.6 V is available for H_2 evolution on p-Si and an η of 1.8 and 1.3 V for O_2 generation on WO_3 and $BiVO_4$, respectively. Furthermore, $BiVO_4$ and WO_3 can only provide theoretical maximum photocurrent densities of 7 and 5 mA cm^{-2}, respectively, suggesting that the photocurrent will be limited by light absorption and charge separation of the photoanode rather than electrocatalysis by $TiNi_{OEC}$ and $TiCo_{OEC}$.

2.2 SSP-coated photoelectrodes and performance

Bifunctionality in water splitting catalysis has only been demonstrated in water electrolysis to date.[10] Here, we explore the utility of composite films from $TiNi_{SSP}$ and $TiCo_{SSP}$ to form protective and bifunctional catalyst layers on state-of-the-art semiconductors in PEC water splitting. While the electrocatalytic activities of the TiNi and TiCo composite films have already been evaluated by electrochemical methods (Figure 3b and Table 1), the coating's success on a semiconductor also strongly depends on the formation of a good interface between the composite and the photoelectrode.[15] A key advantage of our solution-based SSP approach is its simple application to a wide range of substrates by approaches like spin-coating, dropcasting, dip-coating, or inkjet spraying, followed by hydrolytic decomposition under ambient conditions to form a well-interfaced and multi-functional composite layer.

p-Si has been selected as photocathode due to its near-ideal small band gap of 1.1 eV, providing a theoretical photocurrent density of 44 mA cm^{-2}.[3a, 16] WO_3 and $BiVO_4$ are chosen as state-of-the-art photoanodes having band gaps of 2.7 and 2.4 eV, respectively, thus providing respectable photocurrents under solar light irradiation. Additionally, thin films of these n-type semiconductors are easily prepared without requiring arduous procedures (*i.e.* no high temperature annealing above 600 ^{o}C), and exhibit promising water oxidation activity.[7a, 17]

For use in PEC hydrogen evolution, the surface of p-Si must be coated with a protective layer and a HEC in order to prevent quenching of photoactivity due to the rapid formation of SiO_2, and to overcome the kinetic barriers for proton reduction.[7b, 7c] We have previously demonstrated that $TiNi_{SSP}$ acts as a SSP to form a protective TiO_2 layer and a Ni-based HEC on p-Si.[11a] A p-Si|$TiNi_{HEC}$ electrode was prepared by dropcasting a $TiNi_{SSP}$ solution (8 × 30 μL cm^{-2}, 2.5 mM in dry toluene) onto a planar p-Si electrode (0.5 cm^2) followed by cathodic *in situ* activation at E_{appl} = 0 V *vs.* RHE under solar light irradiation in a pH 9.2 B_i solution (Figure S5).[11a]

The p-Si|$TiNi_{HEC}$ displayed a promising photoresponse, with a photocatalytic onset potential (E_{cat}) of 0.3 V *vs.* RHE, close to its valence band edge of 0.5 V *vs.* RHE. A photocurrent density of approximately j = –5.0 mA cm^{-2} was achieved at 0 V *vs.* RHE under solar light irradiation (100 mW cm^{-2}, AM 1.5G) with a quantitative FE (**Figure 4**a, Table 1).[11a] p-Si|$TiCo_{HEC}$ that was formed similarly by dropcasting $TiCo_{pre}$ (8 × 30 μL cm^{-2}, 5 mM in dry toluene) onto p-Si and then activated with the same cathodic *in situ* activation process showed an E_{cat} of only 0.15 V with j = –3.5 mA cm^{-2} at 0 V *vs.* RHE (Figure S5 and S6). Thus, $TiCo_{HEC}$ showed inferior performance compared to $TiNi_{HEC}$ on p-Si and the composite electrode consisting of the latter was employed in PEC water splitting (see below). A bare p-Si electrode does not exhibit meaningful photocurrent at potentials more positive than –0.2 V *vs.* RHE and displays a photocurrent density less than j = –10 μA cm^{-2} at 0 V *vs.* RHE (Figure S5 and S6). Additionally, in the absence of $TiNi_{HEC}$ coating, p-Si lost its activity within minutes. In contrast, $TiNi_{HEC}$ stabilizes p-Si for 4 h with a half-life time of 12 h at 0 V *vs.* RHE. [11a] The physical instability between p-Si and $TiNi_{HEC}$ contributes to longer-term instability, as the catalyst layer visibly detached when vigorous H_2 bubbling was observed.

To analyze the performance of p-Si|$TiNi_{HEC}$ in the bottom-absorber position in a tandem cell, we also recorded the photocurrent with simulated solar light filtered by a TiNi-coated nanostructured WO_3 electrode (nanoWO_3|$TiNi_{OEC}$) and a TiCo-coated nanostructured $BiVO_4$ electrode (nano$BiVO_4$|$TiCo_{OEC}$; see below for more details about the photoanodes). In such a configuration, p-Si|$TiNi_{HEC}$ displays an onset potential of 0.25 V *vs.* RHE and photocurrent densities of approximately j = –3.4 and –3.0 mA cm^{-2} at 0 V *vs.* RHE with the light filtered by nanoWO_3|$TiNi_{OEC}$ and nano$BiVO_4$|$TiCo_{OEC}$, respectively (Figure 4a and S7).

WO_3 is an inexpensive semiconductor material that has a suitable valence band edge (E_{VB} = 3.0 V *vs.* RHE) to provide enough driving force to photooxidize water.[6a, 11c, 18] Nanosheet-structured and monoclinic WO_3 (nanoWO_3) was prepared by a previously reported

hydrothermal method[6a, 11c] and characterized by SEM and p-XRD (**Figure 5**a,b and S8). A key drawback of WO_3 is its chemical instability at pH > 4.[19] However, spin-coating of $TiNi_{SSP}$ (4 × 60 μL cm^{-2}, 5 mM in dry toluene) on nanoWO_3 forms nanoWO_3|$TiNi_{pre}$ with a uniform Ti- and Ni-containing film exhibiting a nanostructured morphology (Figure 5c), which allows it to be employed in neutral-alkaline solution. The sheet thickness was increased from approximately 30 nm to 300 nm after depositing the Ti- and Ni-containing film. $TiNi_{pre}$ is converted *in situ* into $TiNi_{OEC}$, which contains a TiO_2 protection layer and a NiO_x OEC on WO_3.[11c] Illuminated nanoWO_3|$TiNi_{OEC}$ shows an E_{cat} of approximately 0.6 V, a saturation photocurrent density of 0.6 mA cm^{-2} at 1.23 V *vs.* RHE and a FE of 74% at E_{appl} = 1.23 V *vs.* RHE in aqueous pH 9.2 B_i solution (Table 1, Figure 4a).[11c] A $TiCo_{OEC}$ layered nanoWO_3 electrode (nanoWO_3|$TiCo_{OEC}$) was also assembled by the same method, but showed slightly poorer performance than nanoWO_3|$TiNi_{OEC}$ (Figure S9); accordingly, nanoWO_3|$TiNi_{OEC}$ was used in the following tandem cell study.

In the absence of TiNi coating, nanoWO_3 lost 50% of its initial photocurrent within 1 h at 0.94 V *vs.* RHE in pH 9.2 B_i solution. In contrast, nanoWO_3|$TiNi_{OEC}$ shows a half-life time of 4 h under the same conditions, demonstrating the composite film's role as protection layer.[11c] In addition, the TiNi coating enhances the photocurrents of nanoWO_3 in the low bias region (<1.15 V *vs.* RHE, Figure S9). Thus, nanoWO_3|$TiNi_{OEC}$ serves as a suitable photoanode to pair with p-Si|$TiNi_{HEC}$ in pH 9.2 solution in tandem PEC studies. We note that the $TiNi_{OEC}$ coating likely does not fully prevent WO_3 from direct contact with alkaline solution, contributing to the deactivation of nanoWO_3|$TiNi_{OEC}$ on longer time scales. We also note that the lifetime of our protected photoelectrodes is less than that of that of the top-performing TiO_2 passivated electrodes prepared by ALD technique,[7d] which yields much denser and more conformal protective coatings compared to the sol-gel processed SSP chemistry employed here. With further studies, including tuning the molecular ligand and applying a

self-assembly strategy to immobilize a mono-layer of the SSP onto the electrode before decomposition, a more conformal coating may be achieved and provide better surface protection functions.

$BiVO_4$ has a smaller band gap and thus a higher theoretical photocurrent density than WO_3.[2c, 7a, 20] $BiVO_4$ also has a more negative conduction band potential (E_{CB} = +0.1 V *vs.* RHE) than WO_3 (E_{CB} = +0.4 V *vs.* RHE), which should provide a higher photovoltage and operating photocurrent when paired with p-Si in a tandem PEC cell. Key drawbacks of $BiVO_4$ are poor carrier mobility and slow water oxidation kinetics, though near-complete suppression of surface recombination by electrodeposited amorphous CoO_x on $BiVO_4$ has been recently demonstrated.[4d] Thus, we were particularly interested in the effect of $TiCo_{OEC}$ on $BiVO_4$.

Monoclinic scheelite $BiVO_4$ was synthesized by a combined electrochemical deposition/metal-organic decomposition synthesis as reported[7a] and characterized by SEM and p-XRD (Figure 5d,e and S10); the nanoporous structure (nano$BiVO_4$) prepared in this manner has been shown to improve performance, purportedly by reducing the required hole diffusion length and enhancing the catalytic surface area. Nano$BiVO_4$|$TiCo_{OEC}$ was prepared by spin-coating a $TiCo_{SSP}$ solution (4 × 20 μL cm^{-2}, 5 mM in dry toluene) onto a nano$BiVO_4$ electrode. No drastic surface morphology change was observed, but the nano$BiVO_4$ appeared to be decorated with an agglomerated Ti- and Co-containing film (Figure 5f). Nano$BiVO_4$|$TiCo_{OEC}$ exhibits an E_{cat} = 0.2 V *vs.* RHE and j = 1.8 mA cm^{-2} at E_{appl} = 1.23 V *vs.* RHE for water oxidation in pH 9.2 B_i solution during irradiation (Figure 4b). Modification of nano$BiVO_4$ photoanode surfaces with $TiCo_{OEC}$ yielded a significant cathodic shift in E_{cat} and a substantial enhancement of the photocurrent compared to bare nano$BiVO_4$ (Figure 4b and S11). Comparing this composite photoelectrode performance to that of bare nano$BiVO_4$ in PEC experiments with Na_2SO_3 as a hole scavenger reveals that interfacing $TiCo_{OEC}$ with nano$BiVO_4$ almost completely eliminates losses due to surface electron-hole recombination.

A FE of 78% was observed at E_{appl} = 1.23 V *vs.* RHE for nanoBiVO$_4$|TiCo$_{OEC}$ (Table 1 and Figure S12). A TiNi$_{OEC}$ catalytic film also helps suppress the surface charge recombination of BiVO$_4$,[6d, 7a, 21] but is less effective than TiCo$_{OEC}$ (Figure 4b).

The catalytic performance of the TiCo$_{OEC}$ composite layer on nanoBiVO$_4$ appears to compare favorably to that of a recently reported dual-layer FeOOH|NiOOH OEC cocatalyst, in which surface electron-hole recombination is not completely suppressed.[7a] NanoBiVO$_4$|TiCo$_{OEC}$ also functions well in a neutral P$_i$ solution (0.5 M, pH 7) and shows similar performance compared to nanoBiVO$_4$|CoO$_x$-P$_i$, which was prepared by photo-assisted deposition of CoO$_x$ on a nanoBiVO$_4$ electrode from a P$_i$ buffer solution containing 0.5 mM Co(NO$_3$)$_2$ (Figure S13).[4d] However, compared to this (photo)electrodeposition method, the SSP approach reported here offers a better metal-atom efficiency to produce the layer and a higher potential for large scale production of CoO$_x$ OECs by low-temperature inkjet spraying or roll-to-roll processing (*i.e.* for conductive polymer substrates). The dissolution of thin CoO$_x$ layer in a buffer solution during PEC measurements has been recently demonstrated[22] and might be the reason that TiCo$_{OEC}$ shows negligible effect on the stability of nanoBiVO$_4$.

2.3 Tandem PEC cells for overall solar water splitting

Developing a PEC water splitting device that operates in a near pH-neutral environment is desirable in order to extend the range of potential light absorber and catalyst pairs to those that are not stable under strongly acidic and alkaline conditions.[14a] Additionally, operating at moderate pH allows for the use of natural water resources (including sea water)[23] and avoids the handling of corrosive solutions. The mass transport limitations imposed by the lack of H^+ and OH^- ions in these conditions can be overcome by adding supporting electrolyte and by employing circulating electrolyte systems for the forced convection of ionic species.[24] With these considerations in mind, our composite photoelectrode arrays were employed in neutral-

alkaline conditions, minimizing the mass-transport limitations without compromising much photoelectrode performance.

The tandem PEC cells were subsequently assembled by pairing p-Si|$TiNi_{HEC}$ with nanoWO_3|$TiNi_{OEC}$ (PEC cell **I**) and with nano$BiVO_4$|$TiCo_{OEC}$ (PEC cell **II**) for overall solar-driven (100 mW cm^{-2}, AM 1.5G) water splitting at room temperature (**Figure 6**). A two-compartment cell separated by a Nafion^{TM} 117 membrane was used with photoelectrodes having geometric surface areas of approximately 0.5 cm^2, in order to minimize efficiency losses due to the solution or material resistance. Since the photoanodes both have larger band gaps than p-Si, light was first absorbed by these photoanodes (nanoWO_3|$TiNi_{OEC}$ or nano$BiVO_4$|$TiCo_{OEC}$) and the attenuated light then arrived at the back photocathode (p-Si|$TiNi_{HEC}$). Both cells were operated with the photocatalytic surfaces of the two electrodes facing one another, thus optimizing photoanode performance and minimizing ion transport resistances. It is worth noting that we have employed Nafion^{TM} 117 in this study in order to prevent the crossover of the product gases, even though Nafion^{TM} 117 is a proton conducting membrane that does not function ideally in neutral-alkaline conditions. Thus, the device efficiency might be improved if an appropriate alkali anion exchange membrane or glass frit separator is used.

Figure 7 shows the photocurrent density of tandem PEC cell **I** and **II** at applied biases from 0 to 1.23 V in an aqueous B_i solution (0.1 M, pH 9.2) with K_2SO_4 (0.1 M) as supporting electrolyte. An external bias of at least 0.35 V is necessary for tandem PEC Cell **I** to split water, which is consistent with the half-cell performance of p-Si|$TiNi_{HEC}$ placed in tandem cell position and that of nanoWO_3|$TiNi_{OEC}$: an E_{cat} of approximately 0.25 V *vs.* RHE is required for p-Si|$TiNi_{HEC}$ to photoreduce protons, whereas an E_{cat} of 0.6 V *vs.* RHE is needed for nanoWO_3|$TiNi_{OEC}$ to photooxidize water (Figure 4a). In PEC cell **I**, a photocurrent density of approximately 400 μA cm^{-2} is achievable at an applied bias of 0.8 V, close to the expected

required bias of 0.75 V predicted by the half-cell performance of the photoelectrodes (Figure S14); additional required bias to produce this photocurrent density can be accounted for by increased resistance losses incurred in moving to a working two-electrode device.

In the case of PEC cell **II**, a spontaneous, unbiased photocurrent density of 45 ± 18 μA cm^{-2} was observed (Figure 7a) as reasonably predicted from the half-cell performances of p-Si|$TiNi_{HEC}$ and nano$BiVO_4$|$TiCo_{OEC}$ (Figure 4a). A photocurrent density of approximately 1.0 mA cm^{-2} is achievable at an applied bias of 0.6 V in tandem PEC cell **II**, which is also in good agreement with the expected required bias predicted by the half-cell performance of p-Si|$TiNi_{HEC}$ and nano$BiVO_4$|$TiCo_{OEC}$, taking into account some losses in polarization due to resistance (Figure S15).

A first indication of a PEC cell's performance can be determined by calculating the applied bias photon-to-current conversion efficiency (ABPE, **Equation 1**).[1b, 20]

$$\text{ABPE} = \left[\frac{|j| \times (1.23 - V_{bias})}{P_{total}}\right]_{AM1.5G} \quad (1)$$

In this equation, $|j|$ is the photocurrent density (mA cm^{-2}), V_{bias} is the applied bias (V) to the tandem PEC cell, and P_{total} is the energy flux of the illumination (mW cm^{-2}). A maximum ABPE of 0.19 ± 0.01% and 0.65 ± 0.04% was achieved at an applied bias of 0.8 V for PEC Cell **I** and 0.6 V for PEC Cell **II**, respectively (Figure 7b and **Table 2**).

The stability and performance of the cells were subsequently studied at the applied bias where each tandem PEC cell exhibits the highest ABPE. Both tandem PEC cells exhibit respectable lifetime under continuous solar light irradiation, with a half-life time of 2 h and 5 h, respectively; tandem PEC cell **II** also retains 30% of its initial photocurrent after 24 h (Figure 7a, inset). To confirm that the photocurrent of the tandem PEC cell was due to water

splitting, the amount of H_2 and O_2 produced was quantified in the reactor's gaseous headspace by gas chromatography and a fluorescence oxygen probe, respectively (Figure S16). During one hour photoelectrolysis at an external bias of 0.8 V with tandem PEC cell **I**, a charge density of 1.0 ± 0.1 C cm^{-2} passed through the external circuit with 5.0 ± 0.5 μmol cm^{-2} of H_2 and 2.1 ± 0.4 μmol cm^{-2} of O_2 being detected. The corresponding Faradaic efficiencies (FE) are 99% for H_2 and 83% for O_2 (Table 2). In the case of PEC cell **II**, a charge density of 3.3 ± 0.2 C cm^{-2} was generated, with a FE of 91% for H_2 (15.2 ± 0.2 μmol cm^{-2}) and 82% for O_2 (6.9 ± 0.1 μmol cm^{-2}) at an external bias of 0.6 V after one hour of photoelectrolysis (Table 2). The near-quantitative FE and the H_2 to O_2 ratio of approximately 2 to 1 in both tandem cells confirm that the passed charge arises mainly from water splitting.

The measurement of the FE allows us to calculate the true solar to fuel conversion efficiency without relying on the assumption of quantitative product formation. Thus, the 'standalone' solar-to-hydrogen efficiency (STH, **Equation 2**)[20] at zero applied bias can be calculated from the short-circuit photocurrent density (j_{SC}).

$$\text{STH}=\left[\frac{|j_{SC}|\times(1.23)\times(FE)}{P_{total}}\right]_{AM1.5G} \quad (2)$$

PEC cell **I** did not show an unbiased photocurrent, but 45 μA cm^{-2} were generated by PEC cell **II** at zero applied bias corresponding to an STH of 0.05%.

Another meaningful energy conversion efficiency for a working PEC device is the efficiency of solar energy conversion to hydrogen fuel under applied bias conditions (AB-STH, **Equation 3**).[1b, 3b, 25]

$$\text{AB-STH}=\left[\frac{|j|\times(1.23-V_{bias})\times(FE)}{P_{total}}\right]_{AM1.5G} \quad (3)$$

In this calculation, the applied bias is accounted for and only the stored chemical energy from solar photons contributes to the efficiency; hence, performing such an analysis can identify the applied bias at which a working device should be operated for highest efficiency solar-to-fuel conversion. Accordingly, the maximum AB-STH efficiency achieved is 0.19% (at 0.8 V) and 0.59% (at 0.6 V) for tandem PEC cell **I** and **II**, respectively.

2.4 Performance comparison with state-of-the-art tandem PEC cells

Several state-of-the-art tandem cells have been reported, including the "Turner cell" (a $GaInP_2$ photocathode biased by integrated GaAs PV, with an STH efficiency of 12.4%),[4a] an amorphous hydrogenated Si integrated with W doped $BiVO_4$ (3.6%)[4c] and a dye-sensitized solar cell-biased WO_3 (3.1%) or hematite (1.17%).[4b] However, these tandem PEC cells consist of one photoelectrode and one noble metal electrode, and thus are not directly comparable here. An STH efficiency of 8.2% was achieved by side-by-side irradiation of a dual-photoelectrode combination of p-InP and n-GaAs.[26] However, this system also contains very expensive components, and both photoelectrodes were illuminated independently, which means that it is also not fully comparable to our stacked configuration tandem system.

Accordingly, the following discussion focuses on PEC cells consisting of one photoanode and one photocathode in tandem configuration.[3] Recently reported dual photoelectrode tandem PEC cells include Cu_2O paired with WO_3 (Cu_2O-WO_3, AB-STH = 0.11%)[6a], Cu_2O paired with $BiVO_4$ (Cu_2O-$BiVO_4$, STH = 0.5% assuming quantitative FE),[6b] and amorphous Si paired with Fe_2O_3 (aSi-Fe_2O_3, STH = 0.91%)[6c] (Table 3). Cu_2O-$BiVO_4$ and aSi-Fe_2O_3 provide bias-free photocurrent densities of 0.32 mA cm^{-2} and 0.74 mA cm^{-2}, respectively, though the former system employed expensive ALD techniques and the latter used a costly platinum electrocatalyst. Here, tandem PEC cell **II** generates 45 μA cm^{-2} (STH = 0.05%) without an applied bias and achieves an AB-STH efficiency of 0.59%, showing a much better

stability than Cu_2O-$BiVO_4$ (Table 3) without the need for non-scalable techniques and materials. To the best of our knowledge, PEC cell **II**'s AB-STH efficiency is the highest reported solar-to-hydrogen efficiency in a dual-photoelectrode tandem water splitting system that does not employ noble-metal cocatalysts (Table 3).[6-7,14]

2.5 Medium-scale tandem PEC cell

As mentioned above, the success of PEC water splitting devices as a viable technology relies on the scalability of such systems.[27] We have therefore investigated a medium-scale tandem system combining the better-performing nano$BiVO_4$|$TiCo_{OEC}$ photoanode with a p-Si|$TiNi_{HEC}$ photocathode in more detail. Since the measured photocurrent density of nano$BiVO_4$|$TiCo_{OEC}$ was smaller than p-Si|$TiNi_{HEC}$ on the small-scale, this electrode's size was maximized to the greatest allowable illumination area (4 cm^2) in our PEC reactor.

Subsequently, p-Si|$TiNi_{HEC}$ electrodes of different sizes were studied in order to match the overall photocurrent produced by this photocathode to that of the 4 cm^2 photoanode. Ultimately, a 4-to-1 geometric area ratio between the $BiVO_4$ and p-Si electrodes was employed in order to obtain a system with reasonably matched photocurrents over the practically applicable potential range (**Figure 8**a). In half-cell analysis, the p-Si|$TiNi_{HEC}$ with a geometric surface area of 1 cm^2 generated a photocurrent of approximately –2 mA at 0 V *vs.* RHE, whereas nano$BiVO_4$|$TiCo_{OEC}$ with a geometric surface area of 4 cm^2 generated a photocurrent of approximately 3.7 mA at 0.6 V *vs.* RHE. The comparatively reduced photocurrent densities in the larger electrodes are explained by increased *iR* drop in the system due to increased current loads, and by complications in maintaining uniform composite film loadings on the larger surfaces.

In this mid-scale PEC cell **II** where the two photoelectrodes generate comparable photocurrents, the limitation of the two-electrode tandem cell performance is an operating compromise between the photoanode and the photocathode. This mid-scale tandem device

achieved a maximum AB-STH of 0.28%, corresponding to a photocurrent of 1.96 mA at an applied bias of 0.6 V (Figure 8b). In the mid-scale device, an additional 0.2 V of applied bias are required to produce this photocurrent when compared to the expected required bias derived from the photoelectrodes' half-cell performance (Figure S17); this additional device-based overpotential (more noticeable than on the smaller-scale) is attributed to the larger resistive losses resulting from the increased current loads. Nonetheless, a PEC current of almost 2 mA at an applied bias of 0.6 V under standardized solar light irradiation is the highest reported photocurrent (and thus the highest rate of H_2 generation) for a dual photoelectrode PEC water splitting system, to the best of our knowledge.[6a, 6b, 28] While these experiments demonstrate the plausibility of moving toward larger-scale PEC water splitting devices with the current materials, they also serve to highlight some of the challenges that must still be overcome in scaling such systems.

3. Conclusions

In this work, the application of SSP chemistry for preparing multi-functional composite coatings for photoelectrodes has been reported, along with the use of these composite-coated photoelectrodes in PEC water splitting. Ti-/Ni- and Ti-/Co-containing films can be easily and inexpensively prepared by dropcasting or spin-coating SSPs onto a range of conductive and semiconducting substrates under ambient conditions. The TiNi and TiCo films act as precursors to bifunctional HECs and OECs for water splitting in pH 9.2 electrolyte solution, demonstrating compatibility for applying these catalyst films onto water splitting photoelectrodes under the same conditions. In addition to serving as bifunctional electrocatalysts, TiNi and TiCo also act as SSPs to form an amorphous TiO_2 layer for protecting the semiconductor electrodes, thereby enhancing their photostability. We have therefore demonstrated for the first time that a multi-functional material can be integrated

with photoelectrodes for application in solar water splitting, while using an approach that does not require prohibitively expensive or non-scalable materials, techniques, or experimental conditions.

Optimized photocathode and photoanode pairs were subsequently combined and tested in tandem PEC water splitting. Close-to-quantitative H_2 and O_2 gases were generated in a near two-to-one ratio with a benchmark AB-STH efficiency of 0.59% in a PEC cell with p-Si|$TiNi_{HEC}$ wired to nano$BiVO_4$|$TiCo_{OEC}$ in a B_i solution (pH 9.2) at room temperature. By scaling to a mid-sized tandem PEC cell with these electrodes we were able to generate a total photocurrent of approximately 2 mA at an applied bias of 0.6 V, which is believed to be the highest operating photocurrent for a dual photoelectrode PEC device to date. Thus, SSP chemistry has been established for the one-step fabrication of cost-effective, scalable and multi-functional composite materials for PEC water splitting.

4. Experimental Section

Preparation of $TiNi_{SSP}$ and $TiCo_{SSP}$: $TiNi_{SSP}$ and $TiCo_{SSP}$ were synthesized and characterized as reported previously.[12]

Preparation of Electrodes: FTO|$TiNi_{pre}$ and FTO|$TiCo_{pre}$ electrodes were prepared by dropcasting a $TiNi_{SSP}$ (2 x 20 μL, 5 mM in dry toluene) or $TiCo_{SSP}$ precursor solution (2 x 20 μL, 10 mM in dry toluene) onto an FTO-coated glass substrate (Pilkington; TEC Glass™ 7; sheet resistance 7 ohm sq^{-1}, 1 cm^2 exposed surface area). The as-prepared electrodes were then dried in air at room temperature prior to use. FTO|$TiNi_{OEC}$ and FTO|$TiCo_{OEC}$ electrodes were obtained by cycling the electrochemical potential five times between 0.6 and 1.9 V *vs.* RHE with a scan rate of 50 mV s^{-1}. FTO|$TiNi_{HEC}$ and FTO|$TiCo_{HEC}$ electrodes were formed electrolytically in an aqueous B_i solution (0.1 M, pH 9.2) with K_2SO_4 (0.1 M) as supporting electrolyte using E_{appl} = –0.6 V *vs.* RHE for 10 min.

The p-Si photocathodes were prepared from commercial boron-doped Si wafers (University Wafers; resistivity of 1 – 10 ohm cm; (100) single-side polished). The electric contact was formed using a Ga:In eutectic solution (99.99%; Sigma-Aldrich) and a copper wire covered with a conductive silver epoxy resin (RS Components Ltd). The geometric surface area of the photocathodes was defined using Teflon tape (0.5 cm^2) for small-scale PEC measurements and 1 cm^2 for mid-scale PEC measurements. Before the deposition of the electrocatalysts, the silicon surface was cleaned with sequential treatments of H_2O_2 (30 wt% in H_2O; Fisher Scientific), H_2SO_4 (95-98%; Sigma-Aldrich), and HF (65%; Merck Millipore) for 1 min at each step. p-Si|$TiNi_{HEC}$ and p-Si|$TiCo_{HEC}$ were prepared by drop-casting $TiNi_{SSP}$ (30 μL cm^{-2}, 2.5 mM in dry toluene) and $TiCo_{SSP}$ (30 μL cm^{-2}, 5 mM in dry toluene) 8 times onto the Si substrate.

NanoWO_3[6a, 11c] and nano$BiVO_4$[7a] were synthesized following published procedures. NanoWO_3|$TiNi_{OEC}$ and nanoWO_3|$TiCo_{OEC}$ were prepared by spin-coating $TiNi_{SSP}$ (60 μL cm^{-2}, 5 mM in dry toluene) and $TiCo_{SSP}$ (60 μL cm^{-2}, 10 mM in dry toluene) 4 times on the nanoWO_3 substrate, respectively. Nano$BiVO_4$|$TiNi_{OEC}$ and nano$BiVO_4$|$TiCo_{OEC}$ were prepared by spin-coating $TiNi_{SSP}$ (20 μL cm^{-2}, 2.5 mM in dry toluene) and $TiCo_{SSP}$ (20 μL cm^{-2}, 5 mM in dry toluene) 4 times on nano$BiVO_4$, respectively. The geometric surface areas of the photoanodes were defined using a 1350 F polyester tape 3M™ (0.5 cm^2) for PEC measurements and the precise geometric area was determined after the PEC measurements. Mid-scale (approximately 4 cm^2) nano$BiVO_4$|$TiCo_{OEC}$ electrodes were prepared by spin-coating $TiCo_{SSP}$ (5 mM) on nano$BiVO_4$ for 8 cycles.

Electrochemical and PEC measurements: All electrochemical and PEC measurements were recorded with an Ivium CompactStat potentiostat with an electrochemical cell with two compartments separated by a Nafion™ 117 proton exchange membrane. For three-electrode experiments, a Ag/AgCl/KCl_{sat} electrode was employed as the reference electrode and placed

in the same compartment as the working electrode. A platinum foil was used as the counter electrode and was placed in the second compartment. The reported data are not corrected for *iR* drop. Electrode measurements were carried out in a pH 9.2 B_i solution with additional K_2SO_4 (0.1 M) as the supporting electrolyte unless otherwise noted. All redox potentials were converted to RHE by using E (V *vs.* RHE) = E (V *vs.* $Ag/AgCl/KCl_{sat}$) + 0.197 + 0.059×pH.[29] Electrochemical and PEC studies were executed at room temperature.

For tandem PEC cell studies, a two-compartment cell separated by a Nafion™ 117 membrane was used with the photoanode as the front electrode and the photocathode as the back electrode in the same light path. A solar light simulator (Newport Oriel, Xenon 150 W) was used as the light source in all experiments. The light intensity was calibrated to 100 mW cm^{-1} (1 sun). An air mass 1.5 global (AM 1.5G) filter and an IR water filter (to avoid heating of the electrolyte solution) were used.

Physical characterization: SEM was conducted to study the surface morphology of electrodes (Phillips XL30-SFGE). p-XRD analyses were carried out using an X'Pert PRO X-ray diffractometer (PANalytical B.V.). Surface compositions of the electrode were verified by XPS (AXIS Nova, Kratos Analytical, with the CasaXPS software) using a high power monochromatic Al Kα radiation (1486.6 eV, 400 μm spot size, 36 W). Survey spectra were collected with a pass energy of 200 eV and 30 sweeps, whereas high resolution spectra were collected at a pass energy of 40 eV with 10 sweeps.

Hydrogen and Oxygen measurements: Oxygen was analyzed in the headspace of the anodic compartment of the PEC cell using an Ocean Optics fluorescence oxygen probe (FOXY-R). The probe was inserted through a tightly sealed septum and continuous O_2 readings (O_2 partial pressure) at 1 s intervals were made throughout the experiment. For electrocatalytic O_2 production with FTO|$TiCo_{OEC}$, a potential of 2.0 V *vs.* RHE was applied between 0.5 h and 6.5 h of the experiment with the first 0.5 h as control with no applied potential. For PEC O_2

production by nanoBiVO$_4$|TiCo$_{OEC}$ in a three-electrode system, the cell was operated at an applied voltage of 1.23 V *vs.* RHE in the dark during the first 0.5 h (control experiment), followed by 1 h under standardized light illumination (100 mW cm^{-2}) and another 0.5 h in the dark (control experiment). For O_2 quantification in PEC cell **I**, an applied bias of 0.8 V *vs.* RHE was applied in the dark during the first 0.5 h (control experiment), followed by 1 h under illumination and another 0.5 h in the dark (control experiment). In the case of tandem PEC cell **II**, the cell was operated at an applied voltage of 0.6 V *vs.* RHE with the same dark-light-dark intervals. The control experiment is used for determining leakage of O_2 from the atmosphere into the cell and the resulting data was corrected for the derived rate of O_2 leakage. The total amount of O_2 evolved was determined as the sum of O_2 measured in the headspace using the ideal gas law plus dissolved O_2 in the solution calculated by Henry's Law.

The amount of H_2 generated in the headspace of the cathodic compartment was detected and quantified with an Agilent 7890A Series gas chromatography equipped with a 5 Å molecular sieve column (N_2 carrier gas at a flow rate of approximately 3 mL min^{-1}). The gas chromatography oven kept the columns at 45 ^{0}C, and a thermal conductivity detector was used. The electrochemical cell was purged with 2% CH_4 in N_2 for at least 20 min prior to PEC experiments; methane served as an internal standard for H_2 quantification by gas chromatography. Using a syringe, the headspace gas was removed from the airtight electrochemical cell for gas chromatography analysis after electrochemical or PEC experiments. The total amount of H_2 evolved was determined as the sum of H_2 measured in the headspace using the ideal gas law plus dissolved H_2 in the solution calculated by Henry's Law.

Supporting Information

Supporting Information is available from the Wiley Online Library or from the author.

Acknowledgements

Financial support from the Christian Doppler Research Association (Austrian Federal Ministry of Science, Research and Economy and National Foundation for Research, Technology and Development), the OMV Group and the EPSRC (EP/H00338X/2) is gratefully acknowledged. D.W.P. acknowledges support from the Winston Churchill Foundation of the United States. We thank the National EPSRC XPS User's Service (NEXUS) at Newcastle University, an EPSRC Mid-Range Facility for XPS measurements. We acknowledge Dr. Chong-Yong Lee and Dr. Hyun S. Park for their help with the p-Si electrode preparation, Mr. Peter D. Matthews, Mr. Timothy C. King and Prof. Dominic S. Wright for the kind gift of $TiNi_{SSP}$ and $TiCo_{SSP}$ and helpful comments from Dr. Micaela C. Quesada.

Received: ((will be filled in by the editorial staff))
Revised: ((will be filled in by the editorial staff))
Published online: ((will be filled in by the editorial staff))

References

[1] a) J. R. McKone, N. S. Lewis, H. B. Gray, *Chem. Mater.* **2014**, *26*, 407; b) T. Hisatomi, J. Kubota, K. Domen, *Chem. Soc. Rev.* **2014**, *43*, 7520.

[2] a) A. C. Nielander, M. R. Shaner, K. M. Papadantonakis, S. A. Francis, N. S. Lewis, *Energy Environ. Sci.* **2015**, *8*, 16; b) B. A. Pinaud, J. D. Benck, L. C. Seitz, A. J. Forman, Z. Chen, T. G. Deutsch, B. D. James, K. N. Baum, G. N. Baum, S. Ardo, H. Wang, E. Miller, T. F. Jaramillo, *Energy Environ. Sci.* **2013**, *6*, 1983; c) M. S. Prévot, K. Sivula, *J. Phys. Chem. C* **2013**, *117*, 17879.

[3] a) S. Hu, C. Xiang, S. Haussener, A. D. Berger, N. S. Lewis, *Energy Environ. Sci.* **2013**, *6*, 2984; b) J. R. Bolton, S. J. Strickler, J. S. Connolly, *Nature* **1985**, *316*, 495.

[4] a) O. Khaselev, J. A. Turner, *Science* **1998**, *280*, 425; b) J. Brillet, J.-H. Yum, M. Cornuz, T. Hisatomi, R. Solarska, J. Augustynski, M. Grätzel, K. Sivula, *Nat. Photonics* **2012**, *6*, 824; c) F. F. Abdi, L. Han, A. H. M. Smets, M. Zeman, B. Dam, R. van de Krol, *Nat. Commun.* **2013**, *4*, 2195; d) D. K. Zhong, S. Choi, D. R. Gamelin, *J. Am. Chem. Soc.* **2011**, *133*, 18370.

[5] a) C. Liu, J. Tang, H. M. Chen, B. Liu, P. Yang, *Nano Lett.* **2013**, *13*, 2989; b) X. Wang, K.-Q. Peng, Y. Hu, F.-Q. Zhang, B. Hu, L. Li, M. Wang, X.-M. Meng, S.-T. Lee, *Nano Lett.* **2014**, *14*, 18; c) M. R. Shaner, K. T. Fountaine, S. Ardo, R. H. Coridan, H. A. Atwater, N. S. Lewis, *Energy Environ. Sci.* **2014**, *7*, 779.

[6] a) C.-Y. Lin, Y.-H. Lai, D. Mersch, E. Reisner, *Chem. Sci.* **2012**, *3*, 3482; b) P. Bornoz, F. F. Abdi, S. D. Tilley, B. Dam, R. van de Krol, M. Grätzel, K. Sivula, *J. Phys. Chem. C* **2014**, *118*, 16959; c) J.-W. Jang, C. Du, Y. Ye, Y. Lin, X. Yao, J. Thorne, E. Liu, G. McMahon, J. Zhu, A. Javey, J. Guo, D. Wang, *Nat. Commun.* **2015**, *6*, 7447; d) W. B. Ingler, S. U. M. Khan, *Electrochem. Solid State Lett.* **2006**, *9*, G144; e) H. Wang, T. Deutsch, J. A. Turner, *J. Electrochem. Soc.* **2008**, *155*, F91.

[7] a) T. W. Kim, K.-S. Choi, *Science* **2014**, *343*, 990; b) Y. Chen, P. D. Tran, P. Boix, Y. Ren, S. Y. Chiam, Z. Li, K. Fu, L. H. Wong, J. Barber, *Acs Nano* **2015**, *9*, 3829; c) A. Kargar, J. S. Cheung, C.-H. Liu, T. K. Kim, C. T. Riley, S. Shen, Z. Liu, D. J. Sirbuly, D. Wang, S. Jin, *Nanoscale* **2015**, *7*, 4900; d) S. Hu, M. R. Shaner, J. A. Beardslee, M. Lichterman, B. S. Brunschwig, N. S. Lewis, *Science* **2014**, *344*, 1005.

[8] A. Paracchino, V. Laporte, K. Sivula, M. Grätzel, E. Thimsen, *Nat. Mater.* **2011**, *10*, 456.

[9] B. Seger, T. Pedersen, A. B. Laursen, P. C. K. Vesborg, O. Hansen, I. Chorkendorff, *J. Am. Chem. Soc.* **2013**, *135*, 1057.

[10] a) L.-A. Stern, L. Feng, F. Song, X. Hu, *Energy Environ. Sci.* **2015**, *8*, 2347; b) J. Luo, J.-H. Im, M. T. Mayer, M. Schreier, M. K. Nazeeruddin, N.-G. Park, S. D. Tilley, H. J.

Fan, M. Grätzel, *Science* **2014**, *345*, 1593; c) C. He, X. Wu, Z. He, *J. Phys. Chem. C* **2014**, *118*, 4578; d) S. Cobo, J. Heidkamp, P.-A. Jacques, J. Fize, V. Fourmond, L. Guetaz, B. Jousselme, V. Ivanova, H. Dau, S. Palacin, M. Fontecave, V. Artero, *Nature Mater.* **2012**, *11*, 802; e) N. Jiang, B. You, M. Sheng, Y. Sun, *Angew. Chem. Int. Ed.* **2015**, *54*, 6251; Angew. Chem. **2015**, *127*, 6470.

[11] a) Y.-H. Lai, H. S. Park, J. Z. Zhang, P. D. Matthews, D. S. Wright, E. Reisner, *Chem. Eur. J.* **2015**, *21*, 3919; b) Y.-H. Lai, C.-Y. Lin, Y. Lv, T. C. King, A. Steiner, N. M. Muresan, L. Gan, D. S. Wright, E. Reisner, *Chem. Commun.* **2013**, *49*, 4331; c) Y.-H. Lai, T. C. King, D. S. Wright, E. Reisner, *Chem. Eur. J.* **2013**, *19*, 12943; d) Y.-H. Lai, M. Kato, D. Mersch, E. Reisner, *Faraday Discuss.* **2014**, *176*, 199; e) J. Pfrommer, M. Lublow, A. Azarpira, C. Göebel, M. Lüecke, A. Steigert, M. Pogrzeba, P. W. Menezes, A. Fischer, T. Schedel-Niedrig, M. Driess, *Angew. Chem. Int. Ed.* **2014**, *53*, 5183; *Angew. Chem.* **2014**, *126*, 5283; f) P. W. Menezes, A. Indra, P. Littlewood, M. Schwarze, C. Göebel, R. Schomäcker, M. Driess, *ChemSusChem* **2014**, *7*, 2202.

[12] a) S. Eslava, M. McPartlin, R. I. Thomson, J. M. Rawson, D. S. Wright, *Inorg. Chem.* **2010**, *49*, 11532; b) S. Eslava, F. Hengesbach, M. McPartlin, D. S. Wright, *Chem. Commun.* **2010**, *46*, 4701.

[13] a) B. C. M. Martindale, G. A. M. Hutton, C. A. Caputo, E. Reisner, *J. Am. Chem. Soc.* **2015**, *137*, 6018; b) C. Wombwell, E. Reisner, *Dalton Trans.* **2014**, *43*, 4483; c) M. Dincă, Y. Surendranath, D. G. Nocera, *Proc. Natl. Acad. Sci. U.S.A.* **2010**, *107*, 10337.

[14] a) S. Y. Reece, J. A. Hamel, K. Sung, T. D. Jarvi, A. J. Esswein, J. J. H. Pijpers, D. G. Nocera, *Science* **2011**, *334*, 645; b) C.-Y. Lin, D. Mersch, D. A. Jefferson, E. Reisner, *Chem. Sci.* **2014**, *5*, 4906; c) J. Willkomm, N. M. Muresan, E. Reisner, *Chem. Sci.* **2015**, *6*, 2727; d) Y. Surendranath, M. Dincă, D. G. Nocera, *J. Am. Chem. Soc.* **2009**, *131*, 2615.

[15] H. Ye, H. S. Park, A. J. Bard, *J. Phys. Chem. C* **2011**, *115*, 12464.

[16] K. Sun, S. Shen, Y. Liang, P. E. Burrows, S. S. Mao, D. Wang, *Chem. Rev.* **2014**, *114*, 8662.

[17] a) L. Zhang, C.-Y. Lin, V. K. Valev, E. Reisner, U. Steiner, J. J. Baumberg, *Small* **2014**, *10*, 3970; b) Y. Hou, F. Zuo, A. P. Dagg, J. Liu, P. Feng, *Adv. Mater.* **2014**, *26*, 5043.

[18] C. A. Bignozzi, S. Caramori, V. Cristino, R. Argazzi, L. Meda, A. Tacca, *Chem. Soc. Rev.* **2013**, *42*, 2228.

[19] R. S. Lillard, G. S. Kanner, D. P. Butt, *J Electrochem. Soc.,* **1998**, *145*, 2718.

[20] Z. Chen, T. F. Jaramillo, T. G. Deutsch, A. Kleiman-Shwarsctein, A. J. Forman, N. Gaillard, R. Garland, K. Takanabe, C. Heske, M. Sunkara, E. W. McFarland, K. Domen, E. L. Miller, J. A. Turner, H. N. Dinh, *J. Mater. Res.* **2010**, *25*, 3.

[21] L. Zhang, E. Reisner, J. J. Baumberg, *Energy Environ. Sci.* **2014**, *7*, 1402.

[22] M. Zhong, T. Hisatomi, Y. Kuang, J. Zhao, M. Liu, A. Iwase, Q. Jia, H. Nishiyama, T. Minegishi, M. Nakabayashi, N. Shibata, R. Niishiro, C. Katayama, H. Shibano, M. Katayama, A. Kudo, T. Yamada, K. Domen, *J. Am. Chem. Soc.* **2015**, *137*, 5053.

[23] W. Luo, Z. Yang, Z. Li, J. Zhang, J. Liu, Z. Zhao, Z. Wang, S. Yan, T. Yu, Z. Zou, *Energy Environ. Sci.* **2011**, *4*, 4046.

[24] a) M. A. Modestino, K. A. Walczak, A. Berger, C. M. Evans, S. Haussener, C. Koval, J. S. Newman, J. W. Ager, R. A. Segalman, *Energy Environ. Sci.* **2014**, *7*, 297; b) Meenesh R. Singh, K. Papadantonakis, C. Xiang, N. S. Lewis, *Energy Environ. Sci.* **2015**, *8*, 2760.

[25] D. Mersch, C.-Y. Lee, J. Z. Zhang, K. Brinkert, J. C. Fontecilla-Camps, A. W. Rutherford, E. Reisner, *J. Am. Chem. Soc.* **2015**, *137*, 8541.

[26] R. C. Kainthla, B. Zelenay, J. O' M. Bockris, *J. Electrochem. Soc.* **1987**, *134*, 841.

[27] T. Lopes, P. Dias, L. Andrade, A. Mendes, *Sol. Energ. Mat. Sol.* **2014**, *128*, 399.

[28] J. W. Ager, M. R. Shaner, K. A. Walczak, I. D. Sharp, S. Ardo, *Energy Environ. Sci.* **2015**, DOI: 10.1039/c5ee00457h.

[29] A. J. Bard, L. R. Faulkner, *Electrochemical Methods: Fundamentals and Applications*, 2nd ed., John Wiley & Sons, Inc., NewYork, **2001**.

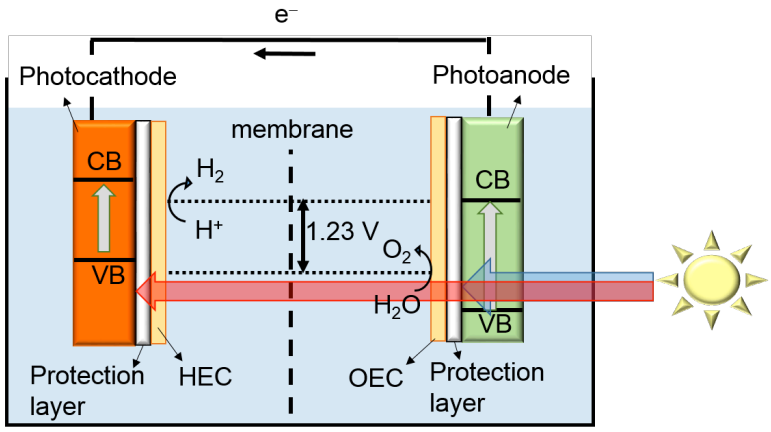

Figure 1. Schematic representation of a tandem PEC cell for solar water splitting consisting of a photocathode integrated with a protection layer and a hydrogen evolution catalyst (HEC) and a photoanode integrated with a protection layer and an oxygen evolution catalyst (OEC). A membrane or separator is used for the separation of the gaseous products.

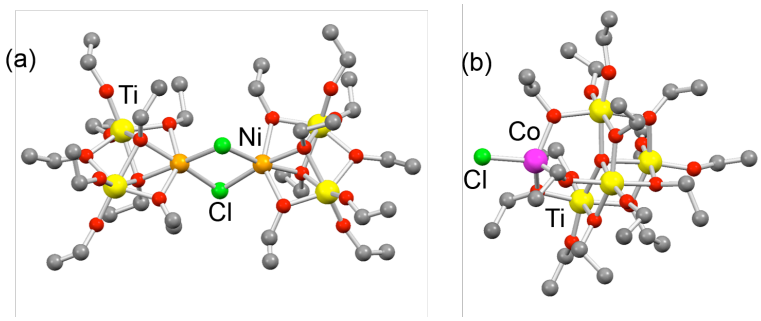

Figure 2. Molecular structure of (a) $[Ti_2(OEt)_9(NiCl)]_2$ $(TiNi_{SSP})$[12a] and (b) $[Ti_4O(OEt)_{15}(CoCl)]$ $(TiCo_{SSP})$[12b] based on crystallographic coordinates (H atoms and disordered ethoxy-groups omitted for clarity): Ti (yellow), Ni (orange), Co (magenta), Cl (green), O (red) and C (grey).

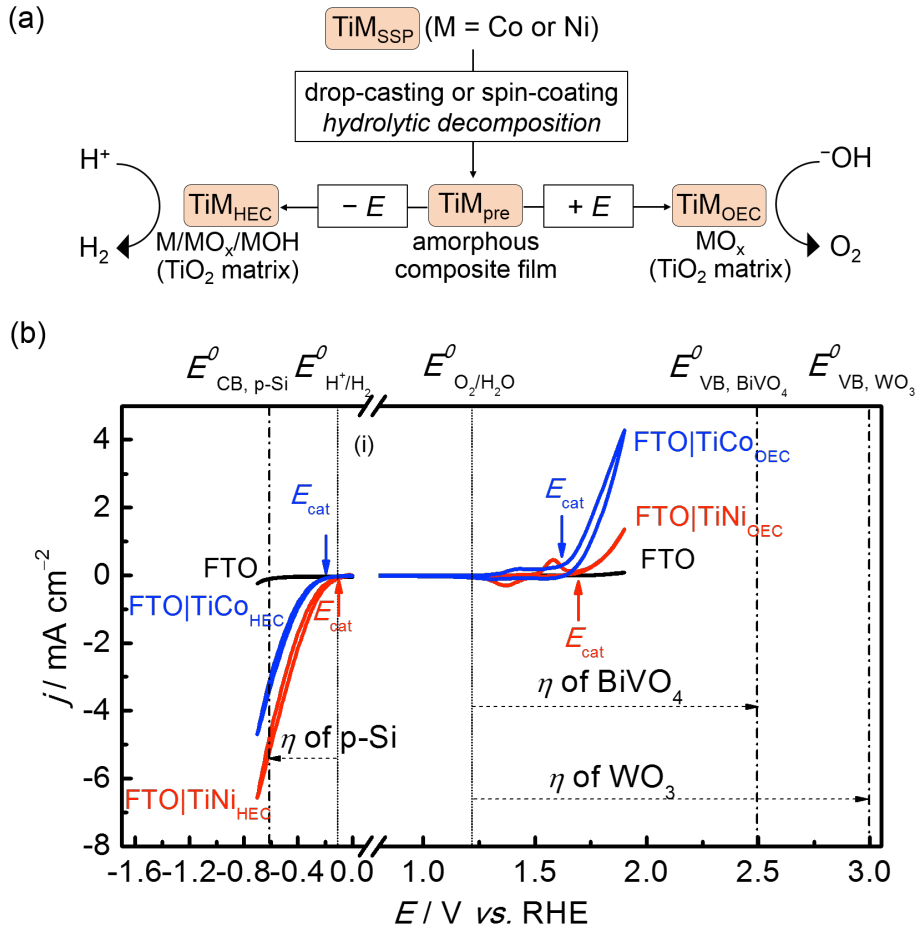

Figure 3. (a) The proposed mechanism of the transformation of $TiNi_{SSP}$ and $TiCo_{SSP}$ to their respective precursor films and bifunctional water splitting catalysts. (b) Cyclic voltammetry (CV) showing the anodic response of FTO|$TiNi_{OEC}$ and FTO|$TiCo_{OEC}$ for water oxidation as well as the cathodic response of FTO|$TiNi_{HEC}$ and FTO|$TiCo_{HEC}$ for proton reduction. Bare FTO is also shown. All CV scans were performed at room temperature in an aqueous electrolyte solution (0.1 M B_i, 0.1 M K_2SO_4, pH 9.2) at a scan rate of 50 mV s^{-1}. FTO|$TiNi_{OEC}$ and FTO|$TiCo_{OEC}$ exhibit an oxidation wave of Ni^{III}/Ni^{II} and Co^{III}/Co^{II} at approximately E_p = 1.58 and 1.41 V *vs*. RHE, respectively.[13c, 14d] *iR* drop is not compensated.

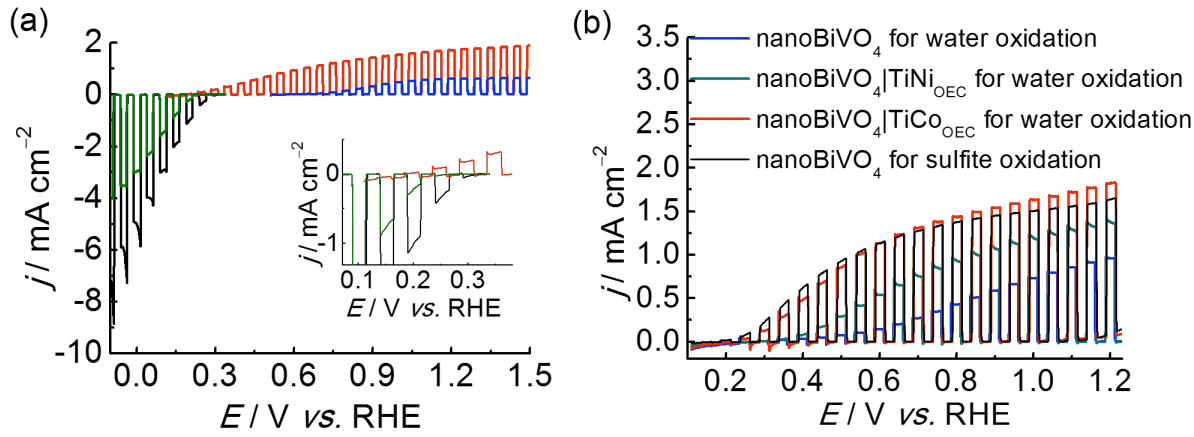

Figure 4. (a) Linear sweep voltammetry (LSV) scans of p-Si|$TiNi_{HEC}$ directly irradiated with chopped light (black trace) and with chopped irradiation filtered by a nanoBiVO$_4$|$TiCo_{OEC}$ electrode (olive). The photoresponse of nanoWO$_3$|$TiNi_{OEC}$ (blue) and nanoBiVO$_4$|$TiCo_{OEC}$ (red) is also shown. Inset magnifies the curve near 0.3 V. (b) LSV scans of nanoBiVO$_4$, nanoBiVO$_4$|$TiNi_{OEC}$, nanoBiVO$_4$|$TiCo_{OEC}$ for water oxidation, and nanoBiVO$_4$ for sulfite oxidation. All measurements were performed in an aqueous pH 9.2 electrolyte solution (0.1 M B_i and 0.1 M K_2SO_4 for water oxidation; 0.1 M B_i and 0.1 M Na_2SO_3 for sulfite oxidation) under chopped solar light irradiation (100 mW cm^{-2}, AM 1.5G) with a scan rate of 5 mV s^{-1}. A Ag/AgCl/KCl_{sat} electrode was employed as the reference electrode, and a Pt foil as the counter electrode; all experiments were conducted at room temperature.

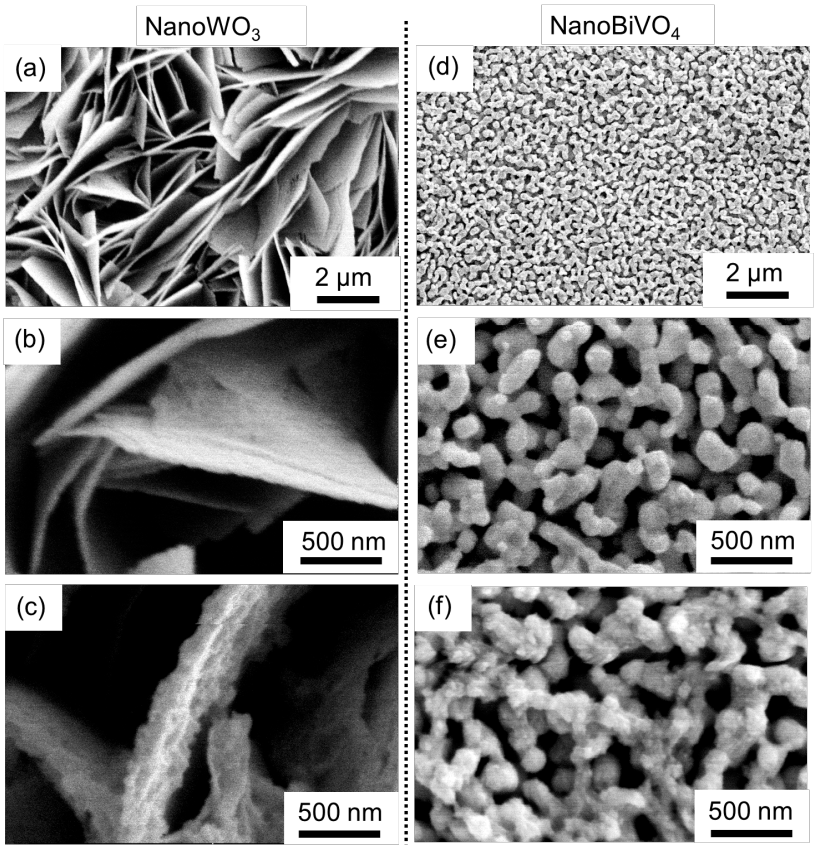

Figure 5. SEM images of (a-b) nanoWO$_3$, (c) nanoWO$_3$|TiNi$_{OEC}$, (d-e) nanoBiVO$_4$, and (f) nanoBiVO$_4$|TiCo$_{OEC}$.

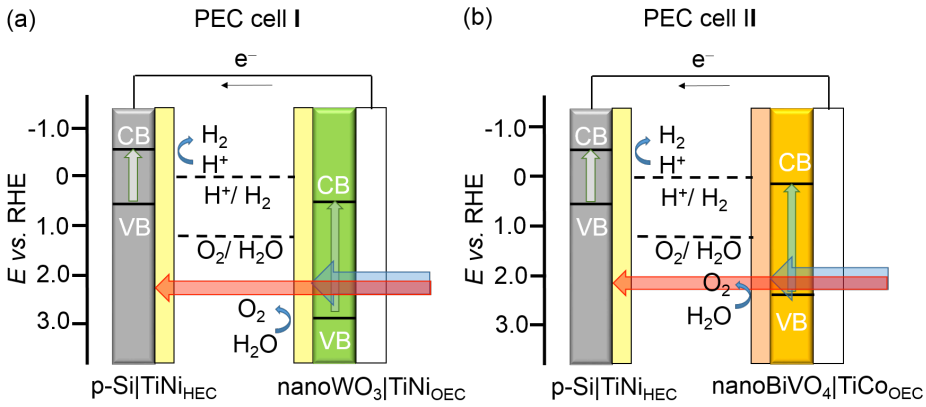

Figure 6. Schematic representation of the tandem PEC cells **I** and **II** for solar water splitting consisting of a p-Si|TiNi$_{HEC}$ photocathode with (a) a nanoWO$_3$|TiNi$_{OEC}$ photoanode and (b) a nanoBiVO$_4$|TiCo$_{OEC}$ photoanode, with the band energies indicated.

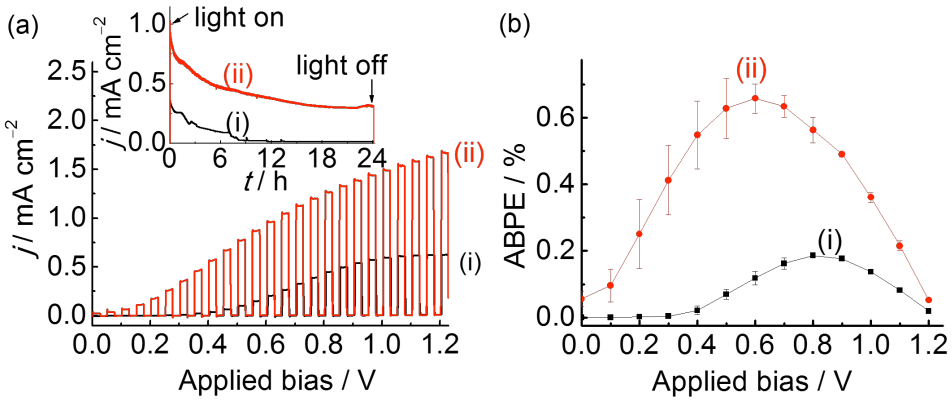

Figure 7. (a) LSV scans under chopped solar light irradiation (100 mW cm^{-2}, AM 1.5G) with a scan rate of 5 mV s^{-1} and (b) the corresponding ABPE of tandem PEC cell **I** (i) and **II** (ii). Inset in (a) shows the chronoamperometric stability of tandem PEC **I** (i) and **II** (ii) recorded at external biases of 0.8 V and 0.6 V, respectively.

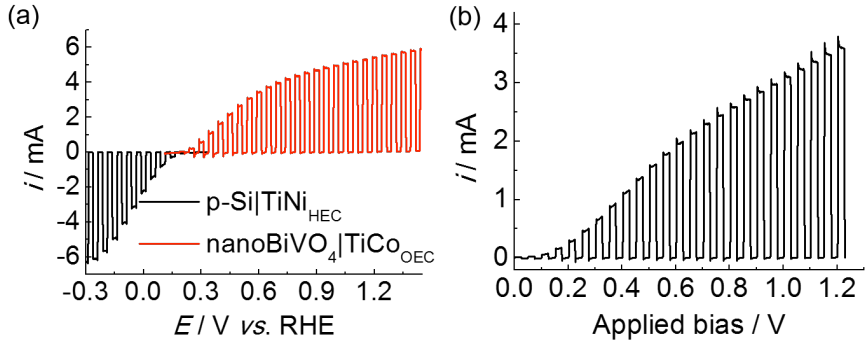

Figure 8. (a) LSV scans of p-Si|$TiNi_{HEC}$ (black, geometric surface area: 1 cm^2) and nanoBiVO_4|$TiCo_{OEC}$ (red, area: 4 cm^2) measured in an aqueous pH 9.2 electrolyte solution (0.1 M B_i and 0.1 M K_2SO_4) with a scan rate of 5 mV s^{-1}. A Ag/AgCl/KCl_{sat} electrode was employed as the reference electrode, and a platinum foil as the counter electrode. The photocurrent of nanoBiVO_4|$TiCo_{OEC}$ was measured under chopped solar light irradiation (100 mW cm^{-2}, AM 1.5G), whereas the photocurrent of p-Si|$TiNi_{HEC}$ was measured in the tandem cell position (illumination filtered by nanoBiVO_4|$TiCo_{OEC}$). (b) LSV scan of tandem PEC cell **II** consisting of a 1 cm^2 p-Si|$TiNi_{HEC}$ and a 4 cm^2 nanoBiVO_4|$TiCo_{OEC}$ under same conditions as (a).

Table 1. Summary of key performance parameters for electro- and photocatalytic H_2 and O_2 production and the corresponding FE in a pH 9.2 B_i (0.1 M) electrolyte solution.

	E_{appl} [V *vs.* RHE]	O_2 or H_2 [μmol h^{-1} cm^{-2}]	FE [%]	Ref
FTO|$TiNi_{OEC}$	2.0	9.8	90	[11c]
FTO|$TiNi_{HEC}$	–0.6	96	97	[11a]
FTO|$TiCo_{OEC}$	2.0	14.3	88	this work
FTO|$TiCo_{HEC}$	–0.6	73	92	this work
WO_3	1.23	0.7	56	[11c]
WO_3|$TiNi_{OEC}$	1.23	2.2	74	[11c]
$BiVO_4$	1.23	N/A[a)]	N/A	this work
$BiVO_4$|$TiCo_{OEC}$	1.23	9.2	78	this work
p-Si	0	N/A	N/A	this work
p-Si|$TiNi_{HEC}$	0	74	100	[11a]

[a)]N/A indicates that the amount of produced gas was below the limit of quantification.

Table 2. Solar water splitting performance of the tandem PEC cells **I** and **II**.

Tandem PEC cell	ABPE [%]	H_2 FE [%]	O_2 FE [%]	STH [%]	AB-STH [%]
I	0.19 ± 0.01[a)]	99 ± 1.8[a)]	83 ± 11[a)]	0	0.19[a)]
II	0.65 ± 0.04[b)]	91 ± 5.3[b)]	82 ± 5.5[b)]	0.05	0.59[b)]

[a)]Applied bias = 0.8 V; [b)]Applied bias = 0.6 V

Table 3. Comparison of key performance parameters in tandem PEC water splitting with paired photoelectrodes.

Tandem PEC cell	ABPE [%]	FE[a)] [%]	STH [%]	AB-STH [%]	Bias [V]	Stability [$t_{1/2}$, min]	Electrolyte solution	Ref
p-Si|$TiNi_{HEC}$ – nanoWO_3|$TiNi_{OEC}$	0.19	99	0	0.19	0.8	120	B_i / K_2SO_4 (pH 9.2)	this work
p-Si|$TiNi_{HEC}$ – nano$BiVO_4$|$TiCo_{OEC}$	0.65	91	0.05	0.59	0.6	300	B_i / K_2SO_4 (pH 9.2)	this work
aSi – Fe_2O_3[b)]	N/A	~100	0.91	N/A	0	>600	P_i (pH 11.8)	[6c]
Cu_2O – WO_3[c)]	0.22	50	0.04	0.11	0.6	N/A	Na_2SO_4 (pH ~ 6)	[6a]
Cu_2O – $BiVO_4$[d)]	N/A	N/A	0.5[e)]	N/A	0	< 20	Na_2SO_4 / P_i (pH 6)	[6b]
$GaInP_2$ – WO_3	N/A	N/A	0.0025[f)]	N/A	0	N/A	H_2SO_4 (3 M)	[6e]
$GaInP_2$ – Fe_2O_3	N/A	N/A	0.00022[f)]	N/A	0	N/A	KNO_3 / P_i (pH 5.7)	[6e]
p-Fe_2O_3 – n-Fe_2O_3	N/A	N/A	0.11[e)]	N/A	0	N/A	H_2SO_4 (0.1 M)	[6d]
Si – TiO_2[g)]	N/A	91	0.12[h)]	N/A	0	N/A	H_2SO_4 (0.5 M)	[5a]

[a)] FE based on H_2 evolution. [b)] Pt is used as a HEC. [c)] A HEC of NiO_x was integrated with nanostructured Cu_2O. [d)] The complete composition of Cu_2O is FTO/Au/Cu_2O/Al:ZnO/TiO_2/RuO_x, where TiO_2 was prepared by ALD and RuO_2 acts as a HEC. [e)] H_2 and O_2 were not quantified and STH was calculated based on the photocurrent measured at 0 bias. [f)] Unbiased photocurrent only observed at > 2 Sun illumination (200 mW cm^{-2}), data shown for 10 Sun. [g)] A fully integrated system of nanostructures with Pt as a HEC and IrO_x as an OEC. h) data shown for 1.5 Sun.

The table of contents entry

Scalable multi-functional composite films are prepared from simple single source precursor chemistry using solely inexpensive materials and techniques. The films provide protection and the integration of bifunctional water splitting catalysts onto photoelectrodes, thus enabling the assembly of a low-cost photoelectrochemical tandem device with a benchmark performance.

Keyword: Photocatalysis

Yi-Hsuan Lai, David W. Palm and Erwin Reisner*

Multi-functional Coatings from Scalable Single Source Precursor Chemistry in Tandem Photoelectrochemical Water Splitting